

Entropy Polarity in Reinforcement Fine-Tuning: Direction, Asymmetry, and Control

Jiazheng Zhang*, Ziche Fu*, Junrui Shen*, Yunbin Zhao*, Yunke Zhang*, Zhiheng Xi, Long Ma, Chenxin An, Zhihao Zhang, Shichun Liu, Dingwei Zhu, Shihan Dou, Shaofan Liu, Han Li, Wiggan Zhou, Aiden Adams, Tao Gui[†], Fei Huang[†], Qi Zhang[†], Xuanjing Huang[†]

Fudan NLP Group, Honor Device Co., Ltd
University of Hong Kong, Shanghai Jiao Tong University and Tencent Hunyuan
jzzhang24@m.fudan.edu.cn, {tgui, qz, xjhuang}@fudan.edu.cn

Policy entropy has emerged as a fundamental measure for understanding and controlling exploration in reinforcement learning with verifiable rewards (RLVR) for LLMs. However, existing entropy-aware methods mainly regulate entropy through global objectives, while the token-level mechanism by which sampled policy updates reshape policy entropy remains underexplored. In this work, we develop a theoretical framework of entropy mechanics in RLVR. Our analysis yields a first-order approximation of the entropy change $\Delta\mathcal{H}$, giving rise to entropy polarity, a signed token-level quantity that predicts how much a sampled update expands or contracts entropy. This analysis further reveals a structural asymmetry: reinforcing frequent high-probability tokens triggers contraction tendencies, whereas expansive tendencies typically require lower-probability samples or stronger distributional correction. Empirically, we show that entropy polarity reliably predicts entropy changes, and that positive and negative polarity branches play complementary roles in preserving exploration while strengthening exploitation. Building on these insights, we propose Polarity-Aware Policy Optimization (PAPO), which preserves both polarity branches and implements entropy control through advantage reweighting. With the empirical entropy trajectory as an online phase signal, PAPO adaptively reallocates optimization pressure between entropy-expanding and entropy-contracting updates. Experiments on mathematical reasoning and agentic benchmarks show that PAPO consistently outperforms competitive baselines, while delivering superior training efficiency and substantial reward improvements.

1. Introduction

Reinforcement fine-tuning (RFT) has substantially improved the capabilities of large language models (LLMs) (Guo et al., 2025; Jaech et al., 2024; Sutton and Barto, 1998; Xi et al., 2026a), especially on complex tasks such as mathematics (Shao et al., 2024), coding (Anthropic, 2025), and agentic decision-making (Feng et al., 2025; Xi et al., 2025; Zhang et al., 2026a). A pivotal post-training paradigm driving these gains is Reinforcement Learning with Verifiable Rewards (RLVR) (An et al., 2025; Guo et al., 2025; Zhang et al., 2025a), where model behavior is optimized against task-specific objectives through automated correctness verification (Zhang et al., 2026b). Despite the rapid progress of RLVR, the exploration and exploitation trade-off remains a central challenge for RFT: excessive exploitation can prematurely narrow the policy and limit further discovery, whereas insufficient exploitation can slow or destabilize learning (Huang et al., 2026; Liu et al., 2021; Tang et al., 2025).

As a practical proxy for policy behavior, entropy has become a critical proxy for understanding RLVR (Chen et al., 2025b; Cheng et al., 2026; Cui et al., 2025). Recent work has begun to analyze

* Equal contribution. [†] Corresponding authors: Tao Gui, Fei Huang, Qi Zhang, Xuanjing Huang.

RLVR from this perspective, highlighting the role of high-entropy tokens and exploratory reasoning dynamics (Petrenko et al., 2026; Wang et al., 2026). Complementary work has proposed a variety of entropy-aware interventions to mitigate entropy collapse, including entropy regularization (Prabhudesai et al., 2025), clamped bonuses (Shen, 2025), and dynamic clipping (Chen et al., 2026; Xi et al., 2026b) for entropy control. However, an in-depth understanding of entropy mechanics remains unresolved: beyond identifying high-entropy regions or designing heuristic interventions, it is still unclear how policy-gradient updates reshape policy entropy along experience trajectories, how these effects evolve over training, and to what extent they drive RLVR’s performance gains.

To this end, we develop a token-level theory of entropy mechanics for RLVR. Instead of viewing entropy as a global training statistic alone, our framework characterizes the microscopic mechanism linking policy gradient to logit perturbation, next-token probability redistribution, and subsequent policy entropy variation. At context state s_t , we characterize the policy behavior via the token-level entropy change:

$$\Delta\mathcal{H}_t = \mathcal{H}\left(\pi_\theta^{k+1}(\cdot | s_t)\right) - \mathcal{H}\left(\pi_\theta^k(\cdot | s_t)\right), \quad (1)$$

whose sign indicates whether it expands or contracts the policy’s exploratory capacity. We show that $\Delta\mathcal{H}_t$ admits a first-order decomposition into a sampled-token contribution and a state-wise distributional correction. This gives rise to a computable signed quantity, **entropy polarity**, that predicts whether and how much reinforcing a given token will increase or decrease local entropy. The polarity view further reveals an asymmetric property: reinforcing high-probability continuations tends to sharpen the distribution, whereas entropy expansion requires lower-probability samples or stronger distributional correction, explaining why entropy collapse is easier to trigger than to reverse.

Building on the theoretical analysis above, we further connect entropy polarity to practical RLVR training. Section 3.3 demonstrates that entropy polarity reliably predicts measured entropy changes between consecutive steps, confirming it as a behaviorally meaningful token-level signal. Section 4.1 further shows that positive and negative-polarity updates induce distinct dynamics: the former preserve exploratory capacity, while the latter strengthen reward-aligned exploitation. Since neither branch alone is sufficient for stable RL in Figure 2, an effective RFT strategy should therefore keep both branches while controlling their relative influence over training instead of favoring one entropy direction or treating them uniformly.

To this end, we propose PAPO, **Polarity-Aware Policy Optimization** framework that turns entropy polarity from an analytical quantity into a control signal for RFT. Rather than regulating entropy uniformly, PAPO directly manages the competition between entropy-expanding and entropy-contracting updates, dynamically redistributing optimization pressure between the two branches according to their effective polarity and the evolving entropy trajectory. In this way, the method preserves exploratory capacity when entropy collapse is imminent, while restoring reward-aligned exploitation when training needs to consolidate useful behaviors. Extensive experiments validate the effectiveness of PAPO spanning mathematics reasoning and agentic tool-calling. Our method consistently outperforms baselines on both in-distribution and out-of-distribution benchmarks. Overall, our main contributions are:

- We develop a token-level theoretical framework for entropy mechanics in RLVR. This leads to entropy polarity, a computable signed quantity that predicts whether and how much a sampled update tends to expand or contract policy entropy.
- We demonstrate that entropy polarity reliably predicts entropy change in empirical study, making it a behaviorally meaningful signal. Positive and negative polarity play complementary roles: the former preserve exploration, whereas the latter promote exploitation.
- We propose PAPO, an efficient RL method that turns entropy polarity into an online signal for entropy control. By dynamically reweighting token-level advantages, the proposed method achieves

competitive performance on both mathematical reasoning and agentic scenarios.

2. Preliminary

Group Relative Policy Optimization. Given a prompt x , LLM π_θ generates response $\pi_\theta(y | x) = \prod_{t=1}^T \pi_\theta(y_t | s_t)$, $s_t := (x, y_{<t})$ denotes the decoding context. In GRPO, the rollout policy samples a group of G responses $\{y^{(i)}\}_{i=1}^G$, and each response $y^{(i)} = (y_1^{(i)}, \dots, y_{T_i}^{(i)})$ receives a response-level reward $r^{(i)} = r(x, y^{(i)})$. It optimizes the clipped surrogate objective

$$\mathcal{J}_{\text{GRPO}}(\theta) = \frac{1}{G} \sum_{i=1}^G \frac{1}{T_i} \sum_{t=1}^{T_i} \min \left(\rho_{i,t}(\theta) A^{(i)}, \text{clip}(\rho_{i,t}(\theta), 1 - \epsilon, 1 + \epsilon) A^{(i)} \right), \quad (2)$$

where $\rho_{i,t}(\theta) = \frac{\pi_\theta(y_t^{(i)} | s_t^{(i)})}{\pi_{\theta_{\text{old}}}(y_t^{(i)} | s_t^{(i)})}$ is the importance sampling ratio and $A^{(i)} = \frac{r^{(i)} - \text{mean}(\mathbf{R})}{\text{std}(\mathbf{R})}$ denotes the normalized advantages within each group.

Policy Entropy. In RFT, entropy has become a practical indicator of policy uncertainty. For a decoding state s_t , let $p_v = \pi_\theta(v | s_t)$ denote the probability assigned to token $v \in \mathcal{V}$. The local policy entropy and its change between consecutive steps are defined as

$$\mathcal{H}_t := - \sum_{v \in \mathcal{V}} p_v \log p_v, \quad \Delta \mathcal{H}_t := \mathcal{H}(\pi_\theta^{k+1}(\cdot | s_t)) - \mathcal{H}(\pi_\theta^k(\cdot | s_t)). \quad (3)$$

Here π_θ^k and π_θ^{k+1} denote the policies before and after one optimization step. A positive $\Delta \mathcal{H}_t$ indicates that the update locally spreads probability mass over alternative continuations, whereas a negative value indicates local concentration around fewer continuations.

3. Entropy Mechanics

We study entropy mechanics through two complementary quantities. The *intrinsic entropy tendency* $\mathcal{T}(s_t, y_t)$ captures how reinforcing a sampled token would reshape entropy based on the token and distribution alone, while the *entropy polarity* $\mathcal{P}(s_t, y_t, A)$ incorporates the signed training signal and captures the realized first-order entropy effect, including both direction and magnitude.

3.1. A Token-Level View of Entropy Change

We analyze how policy gradient reshapes the next-token entropy. Given a decoding state s_t , consider the next-token policy $\pi_\theta(\cdot | s_t)$, parameterized by softmax logits $z_{s_t, v}$ over $v \in \mathcal{V}$. Suppose token $y_t \in \mathcal{V}$ is sampled from state s_t , and the update induced by policy gradient is from the term $A \log \pi_\theta(y_t | s_t)$, where $A \in \mathbb{R}$ is the associated advantage. For compactness, we write

$$p_v := \pi_\theta(v | s_t), \quad p_t := \pi_\theta(y_t | s_t), \quad \mathcal{H}_t := \mathcal{H}(\pi_\theta(\cdot | s_t)).$$

Proposition 1 (Logit Update Under Policy Gradient). *Under the local softmax policy, one gradient-ascent step on $A \log \pi_\theta(y_t | s_t)$ with step size $\eta > 0$ gives $z'_{s_t, v} = z_{s_t, v} + \eta A (\mathbb{1}[v = y_t] - p_v)$ for all $v \in \mathcal{V}$. Equivalently, $z'_{s_t, y_t} = z_{s_t, y_t} + \eta A (1 - p_t)$, and $z'_{s_t, v} = z_{s_t, v} - \eta A p_v$ for $v \neq y_t$.*

Theorem 1 (First-order Entropy Change via Sampled Updates). *Under the setup of Proposition 1, the entropy change at state s_t satisfies*

$$\Delta \mathcal{H}_t = -\eta A t_1(s_t, y_t) + \eta A t_2(s_t) + O(\eta^2), \quad (4)$$

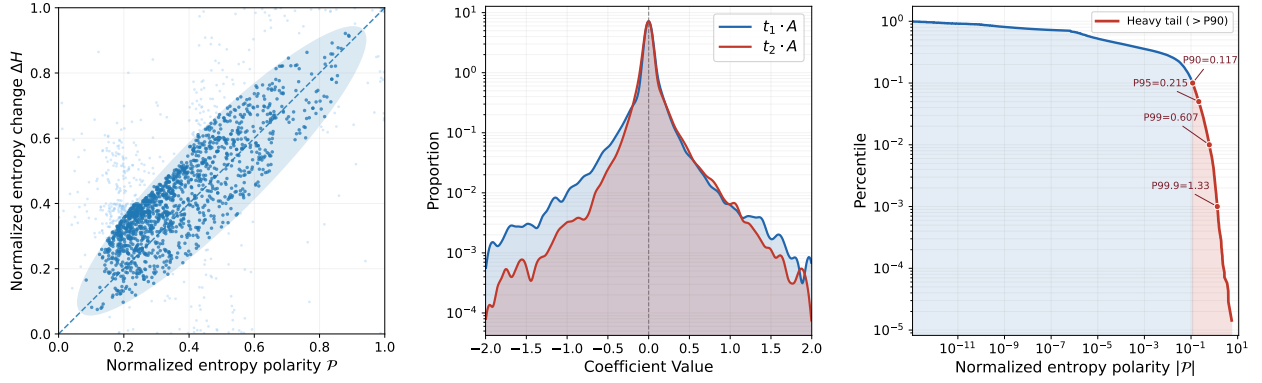


Figure 1 | (a) Correlation between polarity score \mathcal{P} and measured entropy change $\Delta\mathcal{H}$. (b) Histograms for the two decomposed components derived from \mathcal{P} . (c) Percentile curve of the polarity score.

where

$$t_1(s_t, y_t) := p_t(\mathcal{H}_t + \log p_t), \quad t_2(s_t) := \sum_{v \in \mathcal{V}} p_v^2(\mathcal{H}_t + \log p_v). \quad (5)$$

Proof sketch. We derive the result by applying a first-order Taylor expansion to policy entropy, and incorporating the gradient-induced logit update derived in Proposition 1. Under the softmax parametrization,

$$\frac{\partial \mathcal{H}}{\partial z_{s_t, v}} = -p_v(\mathcal{H}_t + \log p_v), \quad \delta z_{s_t, v} = \eta A(\mathbb{1}[v = y_t] - p_v). \quad (6)$$

Substituting $\delta z_{s_t, v}$ into the first-order expansion of \mathcal{H} and collecting the sampled-token term and the distribution term yields Eq. (4). Full derivations are deferred to Appendix A.

Theorem 1 shows that the first-order entropy change induced by a sampled token update factorizes into the signed training signal A and an A -independent token-state quantity $-t_1(s_t, y_t) + t_2(s_t)$. We therefore take this combination as the mechanism-level object of our analysis.

Definition 1 (Intrinsic Entropy Tendency). For a sampled token-state pair (s_t, y_t) , we define

$$\mathcal{T}(s_t, y_t) := -t_1(s_t, y_t) + t_2(s_t). \quad (7)$$

Here, \mathcal{T} measures the entropy tendency induced by positively reinforcing y_t at state s_t : $\mathcal{T} > 0$ indicates entropy expansion, while $\mathcal{T} < 0$ indicates entropy contraction. Because it is independent of the signed advantage, \mathcal{T} characterizes the mechanism-level structure before the actual RL update direction is applied.

3.2. Intrinsic Entropy Tendency and Asymmetry

Recall that the intrinsic entropy tendency is $\mathcal{T}(s_t, y_t) = -t_1(s_t, y_t) + t_2(s_t)$, which combines a sampled-token effect and a state-wise distributional correction. The distributional term $t_2(s_t)$ is shared by all sampled tokens at the same state and acts as a correction toward entropy expansion; it is always non-negative, as it can be expressed as the covariance between token probabilities and their log-probabilities. The sampled-token term enters with a negative sign: since $t_1(s_t, y_t) = p_t(\mathcal{H}_t + \log p_t)$, its sign is governed by the threshold $p_t = \exp(-\mathcal{H}_t)$. Thus, low-probability tokens make $-t_1$ expansion-aligned, whereas high-probability tokens make $-t_1$ contractive.

This sign structure explains the asymmetry of \mathcal{T} . For low-probability samples, $-t_1$ and t_2 jointly favor expansion. For high-probability samples, $-t_1$ competes against the positive correction t_2 , and

contraction is triggered when the token-specific concentration effect dominates. Because policy sampling encounters high-probability tokens more often, reinforcing already dominant tokens tends to further concentrate the local distribution, making contractive tendencies easier to trigger. Conversely, expansion typically requires lower-probability samples or a sufficiently large correction term.

This asymmetry is structural: it is already encoded in \mathcal{T} before the signed training signal is applied; detailed sign analysis and sampled-scale structure are deferred to Appendix A.3. However, practical RL updates are signed and scaled by the advantage, so structural tendency alone does not yet determine the realized first-order entropy effect of an update.

3.3. Entropy Polarity and Empirical Insights

From tendency to polarity. Because actual RL updates are signed by the advantage, we define the entropy polarity of a sampled update as

$$\mathcal{P}(s_t, y_t, A) := A \mathcal{T}(s_t, y_t), \quad \Delta \mathcal{H}_t = \eta \mathcal{P}(s_t, y_t, A) + O(\eta^2). \quad (8)$$

Thus, \mathcal{P} is the realized first-order entropy effect: positive entropy polarity corresponds to an entropy-expanding update, whereas negative entropy polarity corresponds to an entropy-contracting update.

Entropy polarity tracks measured entropy change. Theorem 1 predicts that the signed first-order entropy change is governed by the entropy polarity $\mathcal{P} = A\mathcal{T}$. As shown in Figure 1(a), normalized \mathcal{P} aligns closely with the measured local entropy movement during RL training, confirming that entropy polarity is a practical token-level predictor of entropy direction under sampled updates. This agreement suggests that \mathcal{P} is not merely an analytical artifact, but a reliable signal for analyzing how sampled updates shape local entropy.

Polarity effects are structured and non-uniform. Figure 1(b) plots the two signed components $t_1 \cdot A$ and $t_2 \cdot A$ that enter the first-order entropy change. Their substantial overlap indicates that, under practical RLVR training, both the sampled-token contribution and the state-wise distributional correction materially shape the realized entropy effect. Figure 1(c) further shows a long-tailed magnitude distribution of \mathcal{P} , where a small fraction of high-magnitude updates accounts for a large share of the cumulative entropy effect.

Together, these results support a two-level view of entropy mechanics: \mathcal{T} captures the intrinsic entropy tendency of a sampled token-state pair, while \mathcal{P} incorporates the signed advantage and captures the realized first-order entropy effect—both direction and magnitude—under actual RL updates.

4. Method

4.1. Motivation: Expansion and Contraction Branches

Positive and negative entropy polarity induce opposite training dynamics. To explore the effect of polarity sign in RL, we conduct a single-polarity ablation of RL (Details are presented in Appendix B.5). Figure 2 shows that retaining only positive polarity updates preserves or expands entropy but weakens reward, whereas retaining only negative polarity updates improves reward early but rapidly contracts entropy and reduces later exploration. This indicates that entropy polarity separates entropy-expanding and entropy-contracting branches, and that neither branch alone supports stable reinforcement fine-tuning.

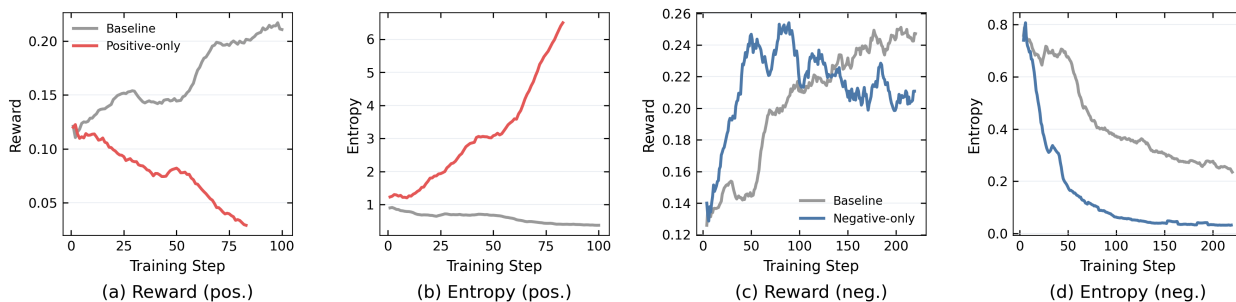


Figure 2 | Ablation study of entropy polarity branches. We retain exclusively positive or negative polarity tokens to compare training dynamics. Positive-polarity updates boost entropy but impair reward learning, whereas negative-polarity updates side unstable optimization and declining entropy.

Characterizing the functional roles of entropy-polarity branches.

To understand this distinction, we inspect tokens from each polarity branch. Quantitatively, Figure 3 shows that positive-polarity tokens are associated with both higher context entropy and greater context diversity, indicating that they tend to occur in more open next-token distributions. We further examine their lexical profiles in Figure 4. Positive-polarity tokens cluster around connective and structural tokens that keep continuations open, whereas negative-polarity tokens concentrate on formulaic reasoning fragments and answer-oriented transitions in more constrained contexts. More discussion about the position concentration of entropy polarity is supplemented in Appendix C.1.

Together, these observations suggest that positive-polarity updates help preserve action diversity, while negative-polarity updates sharpen reward-aligned exploitation.

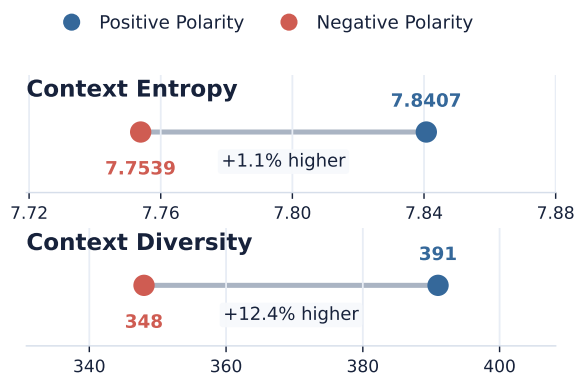


Figure 3 | Contextual statistics of positive and negative polarity.

Motivation for branch-level control. Taken together, these insights indicate complementary roles: **the positive polarity branch preserves exploratory capacity, whereas the negative polarity branch strengthens exploitation.** An effective RFT strategy should therefore keep both branches while controlling their relative influence over training, rather than favoring one entropy direction or treating them uniformly, as in GRPO. Since the desired exploration–exploitation balance changes over time, this control should be adaptive rather than fixed.

4.2. Polarity-Aware Policy Optimization

To this end, we propose **Polarity-Aware Policy Optimization (PAPo)**, which performs branch-level control by reweighting token advantages according to entropy polarity. Rather than targeting a fixed entropy level, PAPo uses the empirical entropy trajectory as an online phase signal to redistribute optimization pressure between entropy-expanding and entropy-contracting updates, protecting exploration when entropy declines rapidly and strengthening exploitation once the trajectory stabilizes.

Table 1 | Performance (%) on in-domain and out-of-domain benchmarks. Cells with deeper background color correspond to better performance within each model group.

Methods	In-Domain Performance						Out-of-Domain		
	Olympiad	AMC	AIME24	AIME25	MATH	Minerva	CRUX	IFEval	MMLU-Pro
<i>Qwen2.5-7B-Base</i>									
- Base	22.30	31.56	4.00	2.00	50.90	17.10	16.25	27.54	36.98
- DAPO	33.12	49.38	13.75	7.50	65.57	24.31	30.63	28.28	37.81
- Ent-Reg	33.08	50.41	12.91	6.70	66.90	25.32	29.75	27.54	37.02
- 80/20	32.69	49.06	16.25	7.08	65.67	24.13	28.62	29.94	36.92
- PAPO	34.70	51.56	14.58	8.30	65.90	26.75	30.88	29.57	37.81
<i>Qwen2.5-14B-Base</i>									
- Base	26.04	36.56	6.67	5.00	56.23	20.77	28.38	30.31	47.33
- DAPO	38.57	60.63	12.50	11.25	70.03	30.93	46.38	33.27	48.00
- Ent-Reg	38.34	58.75	13.75	11.67	71.40	30.83	46.25	33.46	48.15
- 80/20	37.59	59.38	13.33	12.08	69.38	30.88	47.12	33.64	48.25
- PAPO	39.22	62.50	15.83	13.33	71.38	31.94	48.25	33.83	47.89

5. Experiments

5.1. Experimental Setup

Datasets and Models. For the main mathematical reasoning experiments, we train on DAPO-Math-17K (Yu et al., 2026), a widely adopted high-quality RLVR dataset. We use Qwen2.5-7B-Base and Qwen2.5-14B-Base (Yang et al., 2024) as base models, ensuring consistency with baseline comparisons. Additional agentic reasoning experiments use a separate training setup, described in Section 5.3.

Evaluation. To comprehensively assess the model capabilities, we employ a diverse suite of benchmarks encompassing mathematical reasoning, code generation, and general multi-task proficiency. Specifically: (1) Mathematical reasoning: OlympiadBench (He et al., 2024), AMC (Li et al., 2024), MATH500 (Lightman et al., 2024), and AIME (Zhang and Math-AI, 2024); (2) Code generation: CRUX (Gu et al., 2024); (3) Instruction-following and general abilities: IFEval (Zhou et al., 2023) and MMLU-Pro (Wang et al., 2024).

Implementation Details. We implement our algorithms based on the VeRL framework and conduct experiments on $16 \times \text{H20}$ GPUs. During RL training, the learning rate is set to 1×10^{-6} , with a global batch size of 128, and gradient accumulation over 64 steps. For each group, 8 candidate responses are sampled. More implementation illustrations are in Appendix B.4.

5.2. Main Results

Superior performance on mathematical reasoning. Table 1 reports the results of mathematical reasoning on six benchmarks. PAPO achieves state-of-the-art performance on most benchmarks and delivers consistent overall improvements across both 7B and 14B model scales: For Qwen2.5-14B, PAPO outperforms baselines by 3.3% on AIME24 and 2.1% on AIME25; it obtains clear gains of 2.4% on Minerva and 2.2% on AMC on Qwen2.5-7B. Entropy regularization works well on simple benchmarks like MATH500 yet underperforms on challenging competition benchmarks, revealing the limitation of global uniform regularization. Thus PAPO’s token-level polarity-aware reweighting

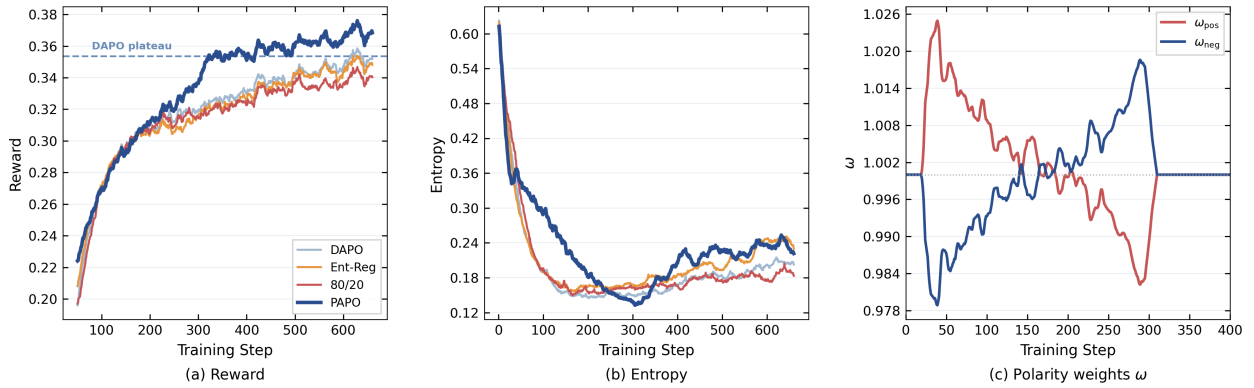


Figure 5 | Training dynamics of PAPO. Reward (left), entropy (middle) and polarity weight (right) of Qwen2.5-14B-Base trained on DAPO-Math-17k. PAPO delivers significant reward improvement while maintaining a healthier entropy dynamic, and its adaptive entropy modulation relaxes back to near-neutral weights after the transient collapse-recovery phase.

provides finer-grained control, yielding more consistent improvements across benchmarks and scales.

PAPO reshapes policy training through phase-adaptive control. Figure 5 shows that PAPO regulates optimization by adaptively rebalancing exploration and exploitation across training phases. In the early stage, the controller prioritizes exploration protection by down-weighting the entropy-contracting branch ($\omega_{neg} < 1$), which helps avoid premature contraction. As entropy decay slows, the controller gradually restores and then mildly favors exploitation ($\omega_{neg} > 1$). After the late-stage gate is triggered, the reweighting is deactivated, and training proceeds with neutral branch weights. This phase-wise control produces a non-monotonic entropy trajectory: PAPO exhibits a transient mid-training contraction, then stabilizes at a higher reward and entropy level than DAPO.

PAPO achieves significant training efficiency. The reward curve in Figure 5 displays significant training efficiency: our method enables the policy model to reach the mature reward performance of DAPO with merely half the training budget, and continues to increase throughout the training stage. Such rapid capability advancement does not stem from over-aggressive early exploitation. As validated by entropy trajectories, the policy preserves strong exploratory capacity, manifesting that the rapid performance growth of our model does not compromise reasoning diversity.

5.3. Analysis

Generalization on out-of-domain benchmarks. We further evaluate the cross-domain generalization of math-optimized checkpoints, including code reasoning (CRUX), instruction following (IFEval), and general knowledge (MMLU-Pro). Despite being trained exclusively on math, PAPO achieves comparable or even superior results over DAPO. For the 14B variant, our method obtains a prominent performance gain of 1.9% on CRUX, verifying that reasoning competencies cultivated via mathematical training can be effectively transferred to code-related understanding tasks. In the 7B setting, PAPO yields a 1.3% improvement on IFEval while maintaining comparable on MMLU-Pro. Our approach achieves desirable improvements without degrading generalization.

Transferability in agentic tool-calling scenarios. We further evaluate PAPO in agentic tool-call generation scenarios, which place high demands on agent-level capabilities such as precise tool intent comprehension and accurate function invocation decision-making, differing from open-ended mathematical reasoning. This setting tests whether polarity-aware reweighting captures a transferable

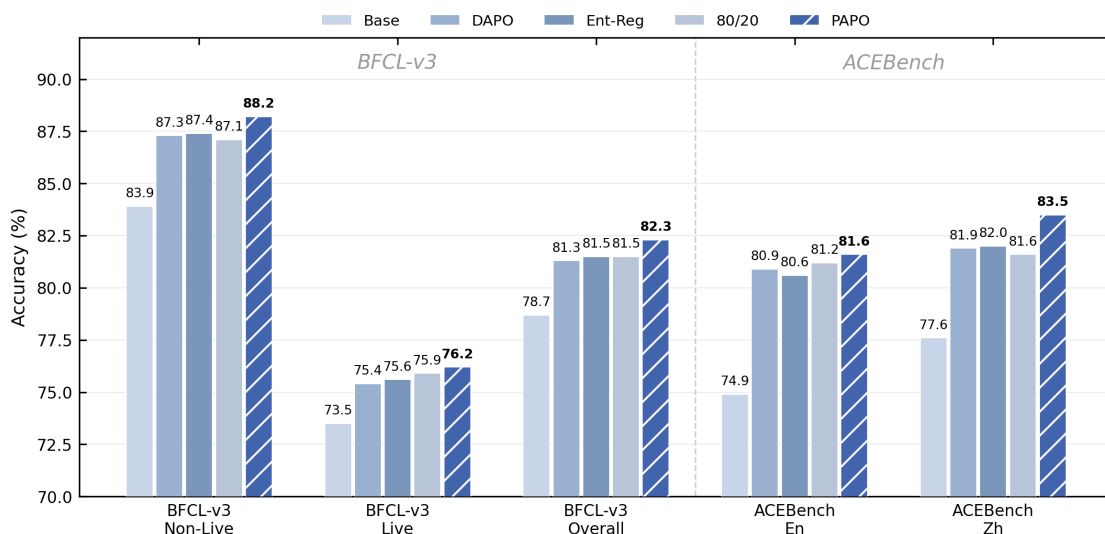


Figure 6 | Performance (%) on agentic tool-using benchmarks. PAPO achieves the strongest overall performance. It consistently surpasses baselines across different evaluation settings, covering non-live and live scenarios in BFCL, as well as English and Chinese tasks in ACEBench.

optimization signal. We train Qwen2.5-14B-Instruct on Tool-N1 (Zhang et al., 2025b) and evaluate on BFCL-v3 (Patil et al., 2025) and ACEBench (Chen et al., 2025a). As shown in Figure 6, PAPO achieves the strongest overall performance among matched methods on both benchmarks, achieving an average +1.0% improvement on BFCL-v3 and the best performance on ACEBench among the compared methods. This suggests that effective-polarity reweighting transfers beyond mathematical reasoning to structured tool-call actions.

Effect of polarity-aware strength on policy dynamics. Figure 7 compares training dynamics with different polarity-control strengths; detailed settings are deferred to Appendix B.6. The exploration-oriented setting preserves entropy more aggressively by suppressing entropy-contracting updates, but consequently weakens the optimization pressure needed for reward improvement, leading to slower gains and a lower final reward. The exploitation-oriented setting exhibits the opposite behavior: reward improves rapidly early on because the contractive branch is less restrained, but this acceleration is achieved at the expense of entropy, inducing premature collapse of exploratory capacity and weaker later-stage improvement. The moderate setting maintains a controlled entropy decline with partial recovery while eventually reaching a competitive reward level. In short, polarity control needs to balance the entropy cost of reward gains, keeping the contractive branch sufficiently robust to sustain learning and avoid premature entropy collapse.

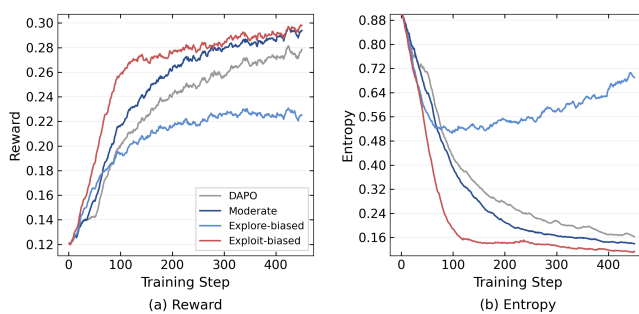


Figure 7 | Effect of polarity-control strength ω on policy dynamics.

6. Related Work

Reinforcement Learning with Verifiable Rewards. RLVR has become a dominant paradigm for improving the reasoning capabilities of large language models (Shao et al., 2024; Zhang et al., 2025a,c), motivating a broad line of work on stable policy optimization. GRPO (Shao et al., 2024) pioneered critic-free optimization for reasoning LLMs, while later methods such as DAPO (Yu et al., 2026) and VAPO (Yu et al., 2026) further improved training stability through refined optimization and value modeling. Subsequent work has explored complementary directions, including scalable training recipes (An et al., 2025; He et al., 2025), sequence-level stabilization for MoE models (Gao et al., 2025; Zheng et al., 2025), and enhanced credit assignment or self-improving training schemes (Bai et al., 2026; Teng et al., 2026).

Entropy Dynamics and Control. Entropy has emerged as a useful lens for understanding exploratory capacity and reasoning behavior in RLVR (Cui et al., 2025; Huang et al., 2026; Meng et al., 2026; Wang et al., 2026; Xi et al., 2026b). Prior work studies entropy dynamics from both analytical and empirical perspectives, showing that RLVR updates often concentrate on a small set of high-impact reasoning tokens (Huang et al., 2026; Meng et al., 2026; Wang et al., 2026). To mitigate entropy collapse, existing methods mainly rely on global or heuristic interventions, including clipping-based trust-region modifications (Chen et al., 2026; Su et al., 2025; Yu et al., 2026) and advantage-shaping or adaptive-control schemes (Chen et al., 2025c; Petrenko et al., 2026). In contrast, our work focuses on how sampled token updates directionally expand or contract entropy, and uses this token-level mechanism to implement entropy control through advantage reweighting.

7. Conclusion, Limitation and Future Work

Conclusion. This work develops a token-level perspective on entropy mechanics in RLVR and introduces intrinsic entropy tendency together with entropy polarity to characterize the directional entropy effect of sampled updates. The resulting framework reveals a structural asymmetry and in turn motivates PAPO, which adaptively modulates the relative influence of the two polarity branches according to the empirical entropy trajectory. Experiments suggest that PAPO provides a practical way to improve the exploration–exploitation trade-off in RLVR.

Limitation and Future Work. This work is restricted to standard RLVR settings with 7B/14B text-LLMs and verifiable reward formulations, and does not yet address long-horizon regimes involving hundreds of sequential reasoning or interaction steps. An important direction for future work is to examine whether the polarity perspective extends to larger-scale models, multimodal scenarios, longer-horizon decision processes, and broader reward formulations.

References

- Chenxin An, Zhihui Xie, Xiaonan Li, Lei Li, Jun Zhang, Shansan Gong, Ming Zhong, Jingjing Xu, Xipeng Qiu, Mingxuan Wang, and Lingpeng Kong. Polaris: A post-training recipe for scaling reinforcement learning on advanced reasoning models, 2025. URL <https://hkunlp.github.io/blog/2025/Polaris>.
- Anthropic. Claude code, 2025. URL [<https://docs.anthropic.com/en/docs/claude-code>] (<https://docs.anthropic.com/en/docs/claude-code>).
- Sikai Bai, Haoxi Li, Jie Zhang, Yongjiang Liu, and Song Guo. Ttvs: Boosting self-exploring reinforcement learning via test-time variational synthesis. *arXiv preprint arXiv:2604.08468*, 2026.

- Chen Chen, Xinlong Hao, Weiwen Liu, Xu Huang, Kingshan Zeng, Shuai Yu, Dexun Li, Shuai Wang, Weinan Gan, Yuefeng Huang, et al. Acebench: Who wins the match point in tool usage? *arXiv preprint arXiv:2501.12851*, 2025a.
- Kun Chen, Peng Shi, Fanfan Liu, Haibo Qiu, Zhixiong Zeng, Siqu Yang, and Wenji Mao. Flexible entropy control in RLVR with gradient-preserving perspective. *CoRR*, abs/2602.09782, 2026. doi: 10.48550/ARXIV.2602.09782. URL <https://doi.org/10.48550/arXiv.2602.09782>.
- Peter Chen, Xiaopeng Li, Ziniu Li, Wotao Yin, Xi Chen, and Tianyi Lin. Exploration vs exploitation: Rethinking RLVR through clipping, entropy, and spurious reward. *CoRR*, abs/2512.16912, 2025b. doi: 10.48550/ARXIV.2512.16912. URL <https://doi.org/10.48550/arXiv.2512.16912>.
- Xinzhu Chen, Xuesheng Li, Zhongxiang Sun, and Weijie Yu. Beyond high-entropy exploration: Correctness-aware low-entropy segment-based advantage shaping for reasoning llms. *CoRR*, abs/2512.00908, 2025c. doi: 10.48550/ARXIV.2512.00908. URL <https://doi.org/10.48550/arXiv.2512.00908>.
- Daixuan Cheng, Shaohan Huang, Xuekai Zhu, Bo Dai, Xin Zhao, Zhenliang Zhang, and Furu Wei. Reasoning with exploration: An entropy perspective. In Sven Koenig, Chad Jenkins, and Matthew E. Taylor, editors, *Fortieth AAAI Conference on Artificial Intelligence, Thirty-Eighth Conference on Innovative Applications of Artificial Intelligence, Sixteenth Symposium on Educational Advances in Artificial Intelligence, AAAI 2026, Singapore, January 20-27, 2026*, pages 30377–30385. AAAI Press, 2026. doi: 10.1609/AAAI.V40I36.40290. URL <https://doi.org/10.1609/aaai.v40i36.40290>.
- Ganqu Cui, Yuchen Zhang, Jiacheng Chen, Lifan Yuan, Zhi Wang, Yuxin Zuo, Haozhan Li, Yuchen Fan, Huayu Chen, Weize Chen, Zhiyuan Liu, Hao Peng, Lei Bai, Wanli Ouyang, Yu Cheng, Bowen Zhou, and Ning Ding. The entropy mechanism of reinforcement learning for reasoning language models. *CoRR*, abs/2505.22617, 2025. doi: 10.48550/ARXIV.2505.22617. URL <https://doi.org/10.48550/arXiv.2505.22617>.
- Lang Feng, Zhenghai Xue, Tingcong Liu, and Bo An. Group-in-group policy optimization for LLM agent training. *CoRR*, abs/2505.10978, 2025. doi: 10.48550/ARXIV.2505.10978. URL <https://doi.org/10.48550/arXiv.2505.10978>.
- Chang Gao, Chujie Zheng, Xionghui Chen, Kai Dang, Shixuan Liu, Bowen Yu, An Yang, Shuai Bai, Jingren Zhou, and Junyang Lin. Soft adaptive policy optimization. *CoRR*, abs/2511.20347, 2025. doi: 10.48550/ARXIV.2511.20347. URL <https://doi.org/10.48550/arXiv.2511.20347>.
- Alex Gu, Baptiste Rozière, Hugh Leather, Armando Solar-Lezama, Gabriel Synnaeve, and Sida I Wang. Cruxeval: a benchmark for code reasoning, understanding and execution. In *Proceedings of the 41st International Conference on Machine Learning*, pages 16568–16621, 2024.
- D Guo, D Yang, H Zhang, J Song, P Wang, Q Zhu, R Xu, R Zhang, S Ma, X Bi, et al. Deepseek-r1 incentivizes reasoning in llms through reinforcement learning. *Nature*, 645(8081):633–638, 2025.
- Bingxiang He, Zekai Qu, Zeyuan Liu, Yinghao Chen, Yuxin Zuo, Cheng Qian, Kaiyan Zhang, Weize Chen, Chaojun Xiao, Ganqu Cui, et al. Justrl: Scaling a 1.5 b llm with a simple rl recipe. *arXiv preprint arXiv:2512.16649*, 2025.
- Chaoqun He, Renjie Luo, Yuzhuo Bai, Shengding Hu, Zhen Thai, Junhao Shen, Jinyi Hu, Xu Han, Yujie Huang, Yuxiang Zhang, et al. Olympiadbench: A challenging benchmark for promoting agi with olympiad-level bilingual multimodal scientific problems. In *Proceedings of the 62nd Annual*

Meeting of the Association for Computational Linguistics (Volume 1: Long Papers), pages 3828–3850, 2024.

Kexin Huang, Haoming Meng, Junkang Wu, Jinda Lu, Chiyu Ma, Ziqian Chen, Xue Wang, Bolin Ding, Jiancan Wu, Xiang Wang, Xiangnan He, Guoyin Wang, and Jingren Zhou. Beyond magnitude: Leveraging direction of RLVR updates for LLM reasoning. In *The Fourteenth International Conference on Learning Representations*, 2026. URL <https://openreview.net/forum?id=r6Pw3RiMYL>.

Aaron Jaech, Adam Kalai, Adam Lerer, Adam Richardson, Ahmed El-Kishky, Aiden Low, Alec Helvar, Aleksander Madry, Alex Beutel, Alex Carney, et al. Openai o1 system card. *arXiv preprint arXiv:2412.16720*, 2024.

Jia Li, Edward Beeching, Lewis Tunstall, Ben Lipkin, Roman Soletskyi, Shengyi Huang, Kashif Rasul, Longhui Yu, Albert Q Jiang, Ziju Shen, et al. Numinamath: The largest public dataset in ai4maths with 860k pairs of competition math problems and solutions. *Hugging Face repository*, 13(9):9, 2024.

Hunter Lightman, Vineet Kosaraju, Yuri Burda, Harrison Edwards, Bowen Baker, Teddy Lee, Jan Leike, John Schulman, Ilya Sutskever, and Karl Cobbe. Let’s verify step by step. In *The Twelfth International Conference on Learning Representations, ICLR 2024, Vienna, Austria, May 7-11, 2024*. OpenReview.net, 2024. URL <https://openreview.net/forum?id=v8LOpN6EOi>.

Evan Zheran Liu, Aditi Raghunathan, Percy Liang, and Chelsea Finn. Decoupling exploration and exploitation for meta-reinforcement learning without sacrifices. In Marina Meila and Tong Zhang, editors, *Proceedings of the 38th International Conference on Machine Learning, ICML 2021, 18-24 July 2021, Virtual Event*, Proceedings of Machine Learning Research, pages 6925–6935. PMLR, 2021. URL <http://proceedings.mlr.press/v139/liu21s.html>.

Haoming Meng, Kexin Huang, Shaohang Wei, Chiyu Ma, Shuo Yang, Xue Wang, Guoyin Wang, Bolin Ding, and Jingren Zhou. Sparse but critical: A token-level analysis of distributional shifts in RLVR fine-tuning of LLMs. In *The Fourteenth International Conference on Learning Representations*, 2026. URL <https://openreview.net/forum?id=8vWIXno8LW>.

Shishir G Patil, Huanzhi Mao, Fanjia Yan, Charlie Cheng-Jie Ji, Vishnu Suresh, Ion Stoica, and Joseph E Gonzalez. The berkeley function calling leaderboard (bfcl): From tool use to agentic evaluation of large language models. In *Forty-second International Conference on Machine Learning*, 2025.

Aleksei Petrenko, Ben Lipkin, Kevin Chen, Erik Wijmans, Marco F. Cusumano-Towner, Raja Giryes, and Philipp Krähenbühl. Entropy-preserving reinforcement learning. *CoRR*, abs/2603.11682, 2026. doi: 10.48550/ARXIV.2603.11682. URL <https://doi.org/10.48550/arXiv.2603.11682>.

Mihir Prabhudesai, Lili Chen, Alex Ippoliti, Katerina Fragkiadaki, Hao Liu, and Deepak Pathak. Maximizing confidence alone improves reasoning. *CoRR*, abs/2505.22660, 2025. doi: 10.48550/ARXIV.2505.22660. URL <https://doi.org/10.48550/arXiv.2505.22660>.

Zhihong Shao, Peiyi Wang, Qihao Zhu, Runxin Xu, Junxiao Song, Xiao Bi, Haowei Zhang, Mingchuan Zhang, YK Li, Yang Wu, et al. Deepseekmath: Pushing the limits of mathematical reasoning in open language models. *arXiv preprint arXiv:2402.03300*, 2024.

Han Shen. On entropy control in LLM-RL algorithms. *CoRR*, abs/2509.03493, 2025. doi: 10.48550/ARXIV.2509.03493. URL <https://doi.org/10.48550/arXiv.2509.03493>.

- Zhenpeng Su, Leiyu Pan, Minxuan Lv, Yuntao Li, Wenping Hu, Fuzheng Zhang, Kun Gai, and Guorui Zhou. CE-GPPO: coordinating entropy via gradient-preserving clipping policy optimization in reinforcement learning. *CoRR*, abs/2509.20712, 2025. doi: 10.48550/ARXIV.2509.20712. URL <https://doi.org/10.48550/arXiv.2509.20712>.
- Richard S. Sutton and Andrew G. Barto. Reinforcement learning: An introduction. *IEEE Trans. Neural Networks*, 9(5):1054–1054, 1998. doi: 10.1109/TNN.1998.712192. URL <https://doi.org/10.1109/TNN.1998.712192>.
- Xinyu Tang, Yuliang Zhan, Zhixun Li, Wayne Xin Zhao, Zhenduo Zhang, Zujie Wen, Zhiqiang Zhang, and Jun Zhou. Rethinking sample polarity in reinforcement learning with verifiable rewards. *CoRR*, abs/2512.21625, 2025. doi: 10.48550/ARXIV.2512.21625. URL <https://doi.org/10.48550/arXiv.2512.21625>.
- Fengwei Teng, Jinyi Bai, Xinhao Yao, Demi Ruohan Wang, Jiahao Zhao, and Zhijiang Guo. Skip-connected policy optimization for implicit advantage. *arXiv preprint arXiv:2604.08690*, 2026.
- Shenzhi Wang, Le Yu, Chang Gao, Chujie Zheng, Shixuan Liu, Rui Lu, Kai Dang, Xiong-Hui Chen, Jianxin Yang, Zhenru Zhang, Yuqiong Liu, An Yang, Andrew Zhao, Yang Yue, Shiji Song, Bowen Yu, Gao Huang, and Junyang Lin. Beyond the 80/20 rule: High-entropy minority tokens drive effective reinforcement learning for LLM reasoning. In *The Thirty-ninth Annual Conference on Neural Information Processing Systems*, 2026. URL <https://openreview.net/forum?id=yfcpdY4gMP>.
- Yubo Wang, Xueguang Ma, Ge Zhang, Yuansheng Ni, Abhranil Chandra, Shiguang Guo, Weiming Ren, Aaran Arulraj, Xuan He, Ziyang Jiang, et al. Mmlu-pro: A more robust and challenging multi-task language understanding benchmark. *Advances in Neural Information Processing Systems*, 37: 95266–95290, 2024.
- Zhiheng Xi, Jixuan Huang, Chenyang Liao, Baodai Huang, Honglin Guo, Jiaqi Liu, Rui Zheng, Junjie Ye, Jiazheng Zhang, Wenxiang Chen, Wei He, Yiwen Ding, Guanyu Li, Zehui Chen, Zhengyin Du, Xuesong Yao, Yufei Xu, Jiecao Chen, Tao Gui, Zuxuan Wu, Qi Zhang, Xuanjing Huang, and Yungang Jiang. Agentgym-rl: Training LLM agents for long-horizon decision making through multi-turn reinforcement learning. *CoRR*, abs/2509.08755, 2025. doi: 10.48550/ARXIV.2509.08755. URL <https://doi.org/10.48550/arXiv.2509.08755>.
- Zhiheng Xi, Xin Guo, Jiaqi Liu, Jiazheng Zhang, Yutao Fan, Zhihao Zhang, Shichun Liu, Mingxu Chai, Xiaowei Shi, Yitao Zhai, Xunliang Cai, Tao Gui, Qi Zhang, and Xuanjing Huang. Can RL improve generalization of LLM agents? an empirical study. *CoRR*, abs/2603.12011, 2026a. doi: 10.48550/ARXIV.2603.12011. URL <https://doi.org/10.48550/arXiv.2603.12011>.
- Zhiheng Xi, Xin Guo, Yang Nan, Enyu Zhou, Junrui Shen, Wenxiang Chen, Jiaqi Liu, Jixuan Huang, Xun Deng, Zhihao Zhang, Honglin Guo, Zhikai Lei, Miao Zheng, Guoteng Wang, Peng Sun, Rui Zheng, Hang Yan, Tao Gui, Qi Zhang, and Xuanjing Huang. BAPO: Stabilizing off-policy reinforcement learning for LLMs via balanced policy optimization with adaptive clipping. In *The Fourteenth International Conference on Learning Representations*, 2026b. URL <https://openreview.net/forum?id=jIeJJqG7dz>.
- An Yang, Baosong Yang, Binyuan Hui, Bo Zheng, Bowen Yu, Chang Zhou, Chengpeng Li, Chengyuan Li, Dayiheng Liu, Fei Huang, Guanting Dong, Haoran Wei, Huan Lin, Jialong Tang, Jialin Wang, Jian Yang, Jianhong Tu, Jianwei Zhang, Jianxin Ma, Jin Xu, Jingren Zhou, Jinze Bai, Jinzheng He, Junyang Lin, Kai Dang, Keming Lu, Keqin Chen, Kexin Yang, Mei Li, Mingfeng Xue, Na Ni, Pei Zhang, Peng Wang, Ru Peng, Rui Men, Ruize Gao, Runji Lin, Shijie Wang, Shuai Bai, Sinan Tan, Tianhang Zhu, Tianhao Li, Tianyu Liu, Wenbin Ge, Xiaodong Deng, Xiaohuan Zhou, Xingzhang

Ren, Xinyu Zhang, Xipin Wei, Xuancheng Ren, Yang Fan, Yang Yao, Yichang Zhang, Yu Wan, Yunfei Chu, Yuqiong Liu, Zeyu Cui, Zhenru Zhang, and Zhihao Fan. Qwen2 technical report. *arXiv preprint arXiv:2407.10671*, 2024.

Qiyang Yu, Zheng Zhang, Ruofei Zhu, Yufeng Yuan, Xiaochen Zuo, YuYue, Weinan Dai, Tiantian Fan, Gaohong Liu, Juncai Liu, LingJun Liu, Xin Liu, Haibin Lin, Zhiqi Lin, Bole Ma, Guangming Sheng, Yuxuan Tong, Chi Zhang, Mofan Zhang, Ru Zhang, Wang Zhang, Hang Zhu, Jinhua Zhu, Jiase Chen, Jiangjie Chen, Chengyi Wang, Hongli Yu, Yuxuan Song, Xiangpeng Wei, Hao Zhou, Jingjing Liu, Wei-Ying Ma, Ya-Qin Zhang, Lin Yan, Yonghui Wu, and Mingxuan Wang. DAPO: An open-source LLM reinforcement learning system at scale. In *The Thirty-ninth Annual Conference on Neural Information Processing Systems*, 2026. URL <https://openreview.net/forum?id=2a36EMSSTp>.

Jiazheng Zhang, Ziche Fu, Zhiheng Xi, Wenqing Jing, Mingxu Chai, Wei He, Guoqiang Zhang, Chenghao Fan, Chenxin An, Wenxiang Chen, Zhicheng Liu, Haojie Pan, Dingwei Zhu, Tao Gui, Qi Zhang, and Xuanjing Huang. Agentv-rl: Scaling reward modeling with agentic verifier, 2026a. URL <https://arxiv.org/abs/2604.16004>.

Jiazheng Zhang, Ziche Fu, Zhiheng Xi, Wenqing Jing, Mingxu Chai, Wei He, Guoqiang Zhang, Chenghao Fan, Chenxin An, Wenxiang Chen, et al. Agentv-rl: Scaling reward modeling with agentic verifier. *arXiv preprint arXiv:2604.16004*, 2026b.

Kaiyan Zhang, Yuxin Zuo, Bingxiang He, Youbang Sun, Runze Liu, Che Jiang, Yuchen Fan, Kai Tian, Guoli Jia, Pengfei Li, Yu Fu, Xingtai Lv, Yuchen Zhang, Sihang Zeng, Shang Qu, Haozhan Li, Shijie Wang, Yuru Wang, Xinwei Long, Fangfu Liu, Xiang Xu, Jiase Ma, Xuekai Zhu, Ermo Hua, Yihao Liu, Zonglin Li, Huayu Chen, Xiaoye Qu, Yafu Li, Weize Chen, Zhenzhao Yuan, Junqi Gao, Dong Li, Zhiyuan Ma, Ganqu Cui, Zhiyuan Liu, Biqing Qi, Ning Ding, and Bowen Zhou. A survey of reinforcement learning for large reasoning models. *CoRR*, abs/2509.08827, 2025a. doi: 10.48550/ARXIV.2509.08827. URL <https://doi.org/10.48550/arXiv.2509.08827>.

Shaokun Zhang, Yi Dong, Jieyu Zhang, Jan Kautz, Bryan Catanzaro, Andrew Tao, Qingyun Wu, Zhiding Yu, and Guilin Liu. Nemotron-research-tool-n1: Exploring tool-using language models with reinforced reasoning. *arXiv preprint arXiv:2505.00024*, 2025b.

Yifan Zhang and Team Math-AI. American invitational mathematics examination (aime) 2024, 2024. Contest problem collection.

Zhihao Zhang, Qiaole Dong, Qi Zhang, Jun Zhao, Enyu Zhou, Zhiheng Xi, Senjie Jin, Xiaoran Fan, Yuhao Zhou, Mingqi Wu, et al. Why reinforcement fine-tuning enables mllms preserve prior knowledge better: A data perspective. *arXiv preprint arXiv:2506.23508*, 2025c.

Chujie Zheng, Shixuan Liu, Mingze Li, Xiong-Hui Chen, Bowen Yu, Chang Gao, Kai Dang, Yuqiong Liu, Rui Men, An Yang, et al. Group sequence policy optimization. *arXiv preprint arXiv:2507.18071*, 2025.

Jeffrey Zhou, Tianjian Lu, Swaroop Mishra, Siddhartha Brahma, Sujoy Basu, Yi Luan, Denny Zhou, and Le Hou. Instruction-following evaluation for large language models. *arXiv preprint arXiv:2311.07911*, 2023.

A. Theoretical Derivations

This appendix provides the full derivations for Proposition 1 and Theorem 1, and further analyzes the sign and magnitude structure of the intrinsic entropy tendency \mathcal{T} . Throughout this appendix,

we fix a decoding state s_t , and write

$$p_\nu := \pi_\theta(\nu | s_t), \quad p_t := \pi_\theta(y_t | s_t), \quad \mathcal{H}_t := - \sum_{\nu \in \mathcal{V}} p_\nu \log p_\nu.$$

All quantities are evaluated at the pre-update policy unless otherwise specified.

A.1. Proof of the Sampled Logit Update

Restatement. For a fixed decoding state s_t , suppose token y_t is sampled and the local policy is updated by the single policy-gradient term $A \log \pi_\theta(y_t | s_t)$ with step size η . Then the first-order logit update satisfies

$$z'_{s_t, \nu} = z_{s_t, \nu} + \eta A (\mathbb{1}[\nu = y_t] - p_\nu), \quad \forall \nu \in \mathcal{V}.$$

Proof. Under the local softmax parameterization,

$$p_\nu = \pi_\theta(\nu | s_t) = \frac{\exp(z_{s_t, \nu})}{\sum_{u \in \mathcal{V}} \exp(z_{s_t, u})}.$$

For the sampled token y_t , we have

$$\log \pi_\theta(y_t | s_t) = z_{s_t, y_t} - \log \left(\sum_{u \in \mathcal{V}} \exp(z_{s_t, u}) \right).$$

Differentiating with respect to $z_{s_t, \nu}$ gives

$$\frac{\partial \log \pi_\theta(y_t | s_t)}{\partial z_{s_t, \nu}} = \mathbb{1}[\nu = y_t] - p_\nu.$$

Therefore,

$$\frac{\partial}{\partial z_{s_t, \nu}} (A \log \pi_\theta(y_t | s_t)) = A (\mathbb{1}[\nu = y_t] - p_\nu).$$

Applying one gradient-ascent step yields

$$z'_{s_t, \nu} = z_{s_t, \nu} + \eta A (\mathbb{1}[\nu = y_t] - p_\nu),$$

which proves Proposition 1. \square

A.2. Proof of the Entropy-Polarity Theorem

Restatement. Under the same local softmax setting, the one-step entropy change induced by the sampled update in Proposition 1 satisfies

$$\Delta \mathcal{H}_t = -\eta A t_1(s_t, y_t) + \eta A t_2(s_t) + O(\eta^2),$$

where

$$t_1(s_t, y_t) := p_t (\mathcal{H}_t + \log p_t), \quad t_2(s_t) := \sum_{\nu \in \mathcal{V}} p_\nu^2 (\mathcal{H}_t + \log p_\nu).$$

Equivalently, with

$$\mathcal{T}(s_t, y_t) := -t_1(s_t, y_t) + t_2(s_t),$$

we have

$$\Delta \mathcal{H}_t = \eta A \mathcal{T}(s_t, y_t) + O(\eta^2).$$

Proof. We first compute the gradient of the local entropy with respect to the logits. Since

$$\mathcal{H}_t = - \sum_{u \in \mathcal{V}} p_u \log p_u,$$

and the softmax derivative satisfies

$$\frac{\partial p_u}{\partial z_{s_t, v}} = p_u(\mathbb{1}[u = v] - p_v),$$

we obtain

$$\begin{aligned} \frac{\partial \mathcal{H}_t}{\partial z_{s_t, v}} &= - \sum_{u \in \mathcal{V}} \frac{\partial p_u}{\partial z_{s_t, v}} (\log p_u + 1) \\ &= - \sum_{u \in \mathcal{V}} p_u (\mathbb{1}[u = v] - p_v) (\log p_u + 1) \\ &= -p_v (\log p_v + 1) + p_v \sum_{u \in \mathcal{V}} p_u (\log p_u + 1). \end{aligned} \quad (12)$$

Using

$$\sum_{u \in \mathcal{V}} p_u (\log p_u + 1) = -\mathcal{H}_t + 1,$$

we have

$$\frac{\partial \mathcal{H}_t}{\partial z_{s_t, v}} = -p_v (\mathcal{H}_t + \log p_v).$$

Let

$$\delta z_{s_t, v} := z'_{s_t, v} - z_{s_t, v}.$$

By the first-order Taylor expansion of entropy around the pre-update logits,

$$\Delta \mathcal{H}_t = \sum_{v \in \mathcal{V}} \frac{\partial \mathcal{H}_t}{\partial z_{s_t, v}} \delta z_{s_t, v} + O(\|\delta z_t\|^2).$$

From Proposition 1,

$$\delta z_{s_t, v} = \eta A (\mathbb{1}[v = y_t] - p_v).$$

Substituting the entropy gradient and the logit update gives

$$\begin{aligned} \Delta \mathcal{H}_t &= -\eta A \sum_{v \in \mathcal{V}} p_v (\mathcal{H}_t + \log p_v) (\mathbb{1}[v = y_t] - p_v) + O(\eta^2) \\ &= -\eta A p_t (\mathcal{H}_t + \log p_t) + \eta A \sum_{v \in \mathcal{V}} p_v^2 (\mathcal{H}_t + \log p_v) + O(\eta^2). \end{aligned} \quad (13)$$

By the definitions in Eq. (5), this becomes

$$\Delta \mathcal{H}_t = -\eta A t_1(s_t, y_t) + \eta A t_2(s_t) + O(\eta^2),$$

which proves Eq. (4).

Using Eq. (7),

$$\mathcal{T}(s_t, y_t) = -t_1(s_t, y_t) + t_2(s_t),$$

we further obtain

$$\Delta \mathcal{H}_t = \eta A \mathcal{T}(s_t, y_t) + O(\eta^2).$$

Together with the definition

$$\mathcal{P}(s_t, y_t, A) = A \mathcal{T}(s_t, y_t)$$

in Eq. (8), this also gives

$$\Delta \mathcal{H}_t = \eta \mathcal{P}(s_t, y_t, A) + O(\eta^2).$$

This completes the proof of Theorem 1. \square

A.3. Sign Analysis and Directional Asymmetry of Entropy Tendency

Theorem 1 shows that the intrinsic entropy tendency is

$$\mathcal{T}(s_t, y_t) = -t_1(s_t, y_t) + t_2(s_t).$$

This section further analyzes how t_1 and t_2 determine the sign and magnitude of \mathcal{T} .

The sampled-token term t_1 . The term

$$t_1(s_t, y_t) = p_t(\mathcal{H}_t + \log p_t)$$

is the only component in \mathcal{T} that depends on the sampled token y_t . Since $p_t > 0$, its sign is fully determined by $\mathcal{H}_t + \log p_t$:

$$\text{sgn}(t_1(s_t, y_t)) = \text{sgn}(\mathcal{H}_t + \log p_t).$$

Therefore,

$$t_1(s_t, y_t) > 0 \iff p_t > \exp(-\mathcal{H}_t),$$

and

$$t_1(s_t, y_t) < 0 \iff p_t < \exp(-\mathcal{H}_t).$$

Thus, t_1 separates sampled tokens by an entropy-induced probability threshold. Tokens above this threshold have a positive t_1 , and hence contribute negatively to \mathcal{T} through the term $-t_1$. Tokens below this threshold have a negative t_1 , and hence contribute positively to \mathcal{T} .

The distribution term t_2 . The term

$$t_2(s_t) = \sum_{v \in \mathcal{V}} p_v^2 (\mathcal{H}_t + \log p_v)$$

does not depend on the sampled token. Instead, it is shared by all sampled-token updates at the same decoding state and depends only on the shape of the local next-token distribution. A useful equivalent form shows that t_2 is always non-negative:

$$\begin{aligned} t_2(s_t) &= \sum_{v \in \mathcal{V}} p_v^2 \log p_v + \mathcal{H}_t \sum_{v \in \mathcal{V}} p_v^2 \\ &= \mathbb{E}_{v \sim p} [p_v \log p_v] - \mathbb{E}_{v \sim p} [p_v] \mathbb{E}_{v \sim p} [\log p_v] \\ &= \text{Cov}_{v \sim p}(p_v, \log p_v) \geq 0. \end{aligned}$$

The last inequality follows because p_v and $\log p_v$ are monotone functions of the same probability value. Therefore, $t_2(s_t)$ acts as a non-negative state-wise distributional correction. Since it enters $\mathcal{T}(s_t, y_t) = -t_1(s_t, y_t) + t_2(s_t)$ with a positive sign, it shifts the intrinsic tendency toward entropy expansion for all sampled tokens at the same state.

Sign analysis of \mathcal{T} . Combining the two terms, the sign of \mathcal{T} is determined by the competition between the sampled-token term t_1 and the distribution term t_2 :

$$\mathcal{T}(s_t, y_t) < 0 \iff t_1(s_t, y_t) > t_2(s_t),$$

and

$$\mathcal{T}(s_t, y_t) > 0 \iff t_1(s_t, y_t) < t_2(s_t).$$

Therefore, when the sampled-token contraction effect t_1 dominates the distributional correction t_2 , the token has a negative intrinsic tendency and tends to decrease local entropy under positive reinforcement. Conversely, when t_2 dominates t_1 , or when $t_1 < 0$, the token has a positive intrinsic

tendency and tends to increase local entropy under positive reinforcement. For negative-advantage updates, the realized direction is reversed by the sign of A , which motivates the effective entropy polarity

$$\mathcal{P}(s_t, y_t, A) = A\mathcal{T}(s_t, y_t).$$

Pointwise asymmetry and realized-scale comparability. The decomposition reveals a subtle distinction between the pointwise form of the intrinsic terms and the empirical scale of the realized components that appear in the entropy change. For a fixed sampled token, the sampled-token term has magnitude

$$|t_1(s_t, y_t)| = p_t |\mathcal{H}_t + \log p_t|,$$

which is pointwise first order in the sampled-token probability p_t , up to the logarithmic factor. The distribution term is

$$t_2(s_t) = \sum_{v \in \mathcal{V}} p_v^2 (\mathcal{H}_t + \log p_v),$$

and therefore aggregates squared-probability contributions over the whole next-token distribution.

This pointwise first-order versus second-order form should not be interpreted as implying that the realized distributional component is negligible in practice. Indeed, under the same policy that generates the sampled token, and for a fixed signed training signal A ,

$$\mathbb{E}_{y_t \sim \pi(\cdot | s_t)} [A t_1(s_t, y_t)] = A \sum_{v \in \mathcal{V}} p_v p_v (\mathcal{H}_t + \log p_v) = A t_2(s_t).$$

Thus, when rollout statistics are collected over sampled token instances, the sampling process itself gives the sampled-token component an additional probability weighting, making the empirical scale of $A t_1$ naturally comparable to that of $A t_2$. This explains why the two realized components can appear on the same order in practice, despite the different pointwise dependence of t_1 and t_2 on token probability.

The resulting asymmetry is therefore directional rather than a universal magnitude dominance. High-probability tokens are sampled more frequently and fall on the contractive side of $-t_1$; when this token-specific concentration effect exceeds the positive correction t_2 , the intrinsic tendency becomes contractive. In contrast, entropy expansion is associated with lower-probability samples or cases where the distributional correction is strong enough to offset the sampled-token concentration effect.

B. Experimental Details

B.1. Pseudo Code of PAPO

To intuitively present the pipeline of PAPO, we summarize the pseudo codes of PAPO in Algorithm 1.

B.2. Evaluation Details

We evaluate across benchmarks spanning mathematical reasoning, code generation, instruction following, and general multi-task abilities.

Mathematical reasoning. We evaluate on six benchmarks: OlympiadBench (He et al., 2024), AMC23 (Li et al., 2024), AIME24, AIME25 (Zhang and Math-AI, 2024), MATH500 (Lightman et al., 2024), and Minerva. For all math benchmarks, answers are extracted from model outputs via rule-based parsing and compared against ground-truth solutions using exact match. In the main table (Table 1), we report mean@8 accuracy: each problem is solved 8 times independently and the average accuracy across all attempts is reported.

Algorithm 1 PAPO: Polarity-Aware Policy Optimization

Require: Policy π_θ ; EMA coefficient β ; bounds $\omega_{\min}, \omega_{\max}$; warmup N_w ; gate ratio γ_{gate}

- 1: $s_0 \leftarrow 0$; $s_{\text{ref}}, h_{\text{ref}} \leftarrow \text{None}$; $\text{active} \leftarrow \text{True}$
- 2: **for** step $k = 1, 2, \dots$ **do**
- 3: Sample responses; compute advantages $A^{(i)}$
- 4: **for all** response i , position t **do** ▷ Polarity
- 5: $\mu \leftarrow \sum_v \pi(v | s_t) \log \pi(v | s_t)$; $t_1 \leftarrow \pi(y_t | s_t) (\log \pi(y_t | s_t) - \mu)$
- 6: $t_2 \leftarrow \sum_v \pi(v | s_t)^2 (\log \pi(v | s_t) - \mu)$; $\mathcal{P}_t^{(i)} \leftarrow A^{(i)} \cdot (-t_1 + t_2)$
- 7: **end for**
- 8: $h_k \leftarrow \text{mean entropy}$; $s_k \leftarrow \beta s_{k-1} + (1-\beta)(h_k - h_{k-1})$
- 9: **if** $k = N_w$ **then** $s_{\text{ref}} \leftarrow s_k$; $h_{\text{ref}} \leftarrow h_k$ ▷ Lock references
- 10: **end if**
- 11: **if active and** $\text{EMA}(h_k) < \gamma_{\text{gate}} h_{\text{ref}}$ **then** $\text{active} \leftarrow \text{False}$ ▷ Deactivate
- 12: **end if**
- 13: **if** $k > N_w$ **and active** **then** ▷ Adaptive weights
- 14: $p_k \leftarrow \text{clip}_{[0,1]} \left(\frac{s_k - s_{\text{ref}}}{-s_{\text{ref}}} \right)$
- 15: $\omega_{\text{neg}} \leftarrow \omega_{\min} + (\omega_{\max} - \omega_{\min}) p_k^2$; $\omega_{\text{pos}} \leftarrow 1/\omega_{\text{neg}}$
- 16: **else** $\omega_{\text{pos}}, \omega_{\text{neg}} \leftarrow 1$
- 17: **end if**
- 18: **for all** response i , position t **do** ▷ Reweight (Eq. (9))
- 19: $\tilde{A}_t^{(i)} \leftarrow A^{(i)} \cdot \omega_{\text{pos}}$ **if** $\mathcal{P}_t^{(i)} > 0$, $A^{(i)} \cdot \omega_{\text{neg}}$ **if** $\mathcal{P}_t^{(i)} < 0$, $A^{(i)}$ **otherwise**
- 20: **end for**
- 21: Update θ via clipped policy gradient with $\tilde{A}_t^{(i)}$
- 22: **end for**

Out-of-domain benchmarks. To assess generalization beyond the math training distribution, we evaluate on three out-of-domain benchmarks: CRUX (Gu et al., 2024) for code reasoning, IFEval (Zhou et al., 2023) for instruction following, and MMLU-Pro (Wang et al., 2024) for general knowledge. CRUX is evaluated via the ZeroEval library; IFEval and MMLU-Pro are evaluated using lm-evaluation-harness. For all OOD benchmarks, we report pass@1 accuracy.

Agentic benchmarks. We evaluate on BFCL-v3 (Patil et al., 2025) and ACEBench (Chen et al., 2025a), reporting accuracy for all results. For BFCL, we follow the official benchmark setup and evaluate on the Live and Non-live subsets while excluding the Multi-turn split. Non-live consists of synthetically generated or curated test cases, whereas Live contains real user-contributed queries. Each subset includes four categories: Simple, Multiple, Parallel, and Parallel Multiple. For ACEBench, we exclude multi-turn cases and focus on two subsets under the Normal category: Atom and Single-turn.

B.3. Baselines

DAPO. DAPO (Yu et al., 2026) serves as the vanilla RLVR baseline. It uses the clip-higher mechanism ($\epsilon_{\text{high}} > \epsilon_{\text{low}}$) to widen the trust region for advantaged tokens, and employs dynamic sampling: for each prompt, more candidate responses are generated than the training batch requires, and prompts whose responses are all correct or all incorrect are filtered out so that only prompts with mixed outcomes contribute to the gradient. DAPO applies no explicit entropy control beyond these mechanisms.

Entropy Regularization. This baseline augments the GRPO objective with an entropy bonus term $\alpha \mathcal{H}(\pi_\theta)$ added to the loss, encouraging the policy to maintain higher entropy throughout training. The regularization is applied uniformly across all tokens regardless of their role in entropy dynamics.

80/20. Following (Wang et al., 2026), this method retains only the top 20% of tokens ranked by per-token entropy and computes the policy gradient exclusively on this high-entropy subset. The motivation is that reasoning-critical tokens concentrate at high-entropy positions; by discarding low-entropy tokens, the gradient signal focuses on the subset most relevant to exploratory reasoning.

B.4. Training Configuration

All math experiments are built on the VeRL framework and trained on $16 \times \text{H20}$ GPUs. We train for 6 epochs with a learning rate of 1×10^{-6} and a sampling temperature of 1.0. The generation batch size is 256; the training batch size is 128 with gradient accumulation over 64 steps. For each prompt, 8 candidate responses are sampled with a maximum completion length of 8,192 tokens. clipping range $[\epsilon_{\text{low}}, \epsilon_{\text{high}}] = [0.2, 0.28]$ follows DAPO, without KL penalty.

For PAPO, the polarity weight bounds are set to $[\omega_{\text{min}}, \omega_{\text{max}}] = [0.98, 1.02]$ for the 14B backbone and $[0.98, 1.03]$ for the 7B backbone. The entropy-slope EMA uses $\beta_{\text{warm}} = 0.95$ during the warmup phase and $\beta_{\text{run}} = 0.9$ thereafter. The warmup phase lasts $N_w = 20$ steps, during which training runs with neutral weights ($\omega_{\text{pos}} = \omega_{\text{neg}} = 1$) to estimate the reference collapse rate s_{ref} . The gate threshold is set to $\gamma_{\text{gate}} = 0.3$: once the smoothed entropy falls below $0.3 \cdot h_{\text{ref}}$, the adaptive reweighting deactivates permanently. All baselines (DAPO, Ent-Reg, 80/20) share the same training budget, batch sizes, and evaluation protocol to ensure a fair comparison.

Agentic experiments are based on Tool-N1 dataset for 7 epochs with a learning rate of 1×10^{-6} and a sampling temperature of 0.7. The generation batch size is 256; the training batch size is 128 with gradient accumulation over 64 steps. Group size is 5 and with a maximum completion length of 8,192 tokens. For PAPO, the polarity weight bounds are set to $[\omega_{\text{min}}, \omega_{\text{max}}] = [0.99, 1.05]$. The entropy-slope EMA uses $\beta_{\text{warm}} = 0.95$ during the warmup phase and $\beta_{\text{run}} = 0.9$ thereafter. The warmup phase lasts $N_w = 25$ steps, during which training runs with neutral weights ($\omega_{\text{pos}} = \omega_{\text{neg}} = 1$) to estimate the reference collapse rate s_{ref} .

B.5. Details of Single-Polarity Ablation

To verify the functional meaning of effective polarity, we conduct the single-polarity ablation shown in Figure 2. For each sampled token update, we compute the effective polarity $\mathcal{P}(s_t, y_t, A) = \mathcal{A}\mathcal{T}(s_t, y_t)$. The positive-only variant keeps token-level policy-gradient terms with $\mathcal{P} > 0$ and masks out terms with $\mathcal{P} < 0$. The negative-only variant keeps terms with $\mathcal{P} < 0$ and masks out terms with $\mathcal{P} > 0$. This diagnostic ablation is implemented on vanilla GRPO rather than the DAPO-based recipe used in the main experiments. This choice isolates the effect of polarity sign and avoids confounding from DAPO-specific sampling or clipping mechanisms and from PAPO’s adaptive reweighting. Apart from this objective choice and the polarity mask, rewards, advantage normalization, and other hyperparameters follow the main math experimental setup.

B.6. Details of Polarity-Aware Strength Ablation

This ablation (Figure 7) examines how the polarity weight bounds $[\omega_{\text{min}}, \omega_{\text{max}}]$ affect the exploration–exploitation trade-off during training. All three PAPO configurations use Qwen2.5-7B-Base on the same math training setup described in Appendix B.4; the only difference is the polarity weight range:

Table 2 | Performance (%) on out-of-domain tasks.

Methods	CRUX			IFEval			MMLU-Pro		
	Pass@1	Pass@5	Pass@10	Pass@1	Pass@5	Pass@10	Pass@1	Pass@5	Pass@10
Qwen-2.5-7B-Base									
Base	16.25	47.00	60.62	27.54	39.56	43.81	36.98	65.33	75.20
DAPO	30.63	61.12	70.38	28.28	53.79	61.18	37.81	70.82	81.83
Ent-Reg	29.75	54.62	66.50	27.54	54.16	62.85	37.02	70.11	82.33
80/20	28.62	60.75	68.25	29.94	52.13	60.26	36.92	69.95	81.92
PAPO	30.88	61.00	69.62	29.57	52.31	60.81	37.81	71.16	82.25
Qwen-2.5-14B-Base									
Base	28.38	60.75	70.12	30.31	58.23	66.91	47.33	77.35	86.12
DAPO	46.38	73.12	80.38	33.27	57.12	67.84	48.00	77.20	86.23
Ent-Reg	46.25	70.75	79.12	33.46	58.04	68.76	48.15	77.84	86.46
80/20	47.12	73.25	78.25	33.64	58.04	66.54	48.25	77.60	86.07
PAPO	48.25	74.62	80.12	33.83	57.12	66.54	47.89	77.65	86.02

- **Explore-biased:** $[\omega_{\min}, \omega_{\max}] = [0.99, 1.06]$. The wider upper bound amplifies the expansion branch while the near-unity lower bound leaves the contraction branch almost unmodified.
- **Exploit-biased:** $[\omega_{\min}, \omega_{\max}] = [0.96, 1.00]$. The sub-unity upper bound prevents any amplification of the expansion branch, while the lower bound actively suppresses it, allowing the contraction branch to dominate.
- **Moderate:** $[\omega_{\min}, \omega_{\max}] = [0.98, 1.03]$. This is the same setting used in the 7B main experiment.

The DAPO baseline shares the same training budget and hyperparameters but applies no polarity reweighting ($\omega_{\text{pos}} = \omega_{\text{neg}} = 1$ throughout).

B.7. Prompt Templates

Math reasoning. All math experiments use the Qwen chat template with the following prompt format:

```
<|im_start|>system
You are a helpful assistant.<|im_end|>
<|im_start|>user
{input}
Please reason step by step, and put your final answer within \boxed{ }.<|im_end|>
<|im_start|>assistant
```

where {input} is replaced by the problem statement from DAPO-Math-17K.

Agentic Reasoning All agentic experiments use the Qwen chat template with the following prompt format:

```

<|im_start|>system
You are an expert in composing functions. You are given a question and a set
of possible functions. Based on the question, you will need to make one or
more function/tool calls to achieve the purpose. If none of the function can
be used, point it out. If the given question lacks the parameters required by
the function, also point it out. You should only return the function call in
tools call sections. Here is a list of functions in JSON format that you can
invoke:
# Tool

You are provided with function signatures within <tools></tools> XML tags:

<tools>
{tools}
</tools>

In each action step, you MUST:
1. Think about the reasoning process in the mind and enclosed your reasoning
within <think></think> XML tags.
2. Then, provide a json object with function names and arguments
within <tool_call></tool_call> XML tags. i.e., <tool_call>[{"name":
<function-name>, "arguments": <args-json-object>}, {"name":
<function-name2>, "arguments": <args-json-object2>}, ...]</tool_call>
3. Make sure both the reasoning and the tool call steps are included together
in one single reply.
A complete reply example is: <think> To address the query, I need to send the
email to Bob and then buy the banana through walmart. </think> <tool_call>
[{"name": "email", "arguments": {"receiver": "Bob", "content": "I will
buy banana through walmart"}}, {"name": "walmart", "arguments": {"input":
"banana"}}]</tool_call>. Please make sure the type of the arguments is
correct.<|im_end|>
<|im_start|>user
{input}
<|im_end|>
<|im_start|>assistant

```

where {tools} and {input} are replaced by the tool list and the problem statement from the Tool-N1 dataset, respectively.

C. Additional Results

C.1. Positional Distribution of Entropy Polarity

We explore how \mathcal{P} varies with token position within each rollout in Figure 8.

Magnitude distribution. The mean $|\mathcal{P}|$ remains nearly constant across all positions (≈ 0.04), while the median sits approximately three orders of magnitude lower ($\sim 10^{-5}$), confirming the heavy-tail sparsity reported in Section 3.3. This gap implies that more than half of all tokens at every position contribute negligibly to entropy dynamics; the entropy-shaping effect is concentrated in a sparse tail of high- $|\mathcal{P}|$ tokens. The median exhibits a mild boundary effect—elevated at the start and end of the rollout ($\sim 10^{-2}$ to 10^{-4}) compared to $\sim 10^{-5}$ in the interior—suggesting that tokens near sequence boundaries carry moderately higher polarity on average. Crucially, however, the flat mean demonstrates that the dominant entropy-shaping tokens are distributed uniformly across all positions. This justifies a position-agnostic reweighting scheme: methods that filter tokens by position would discard

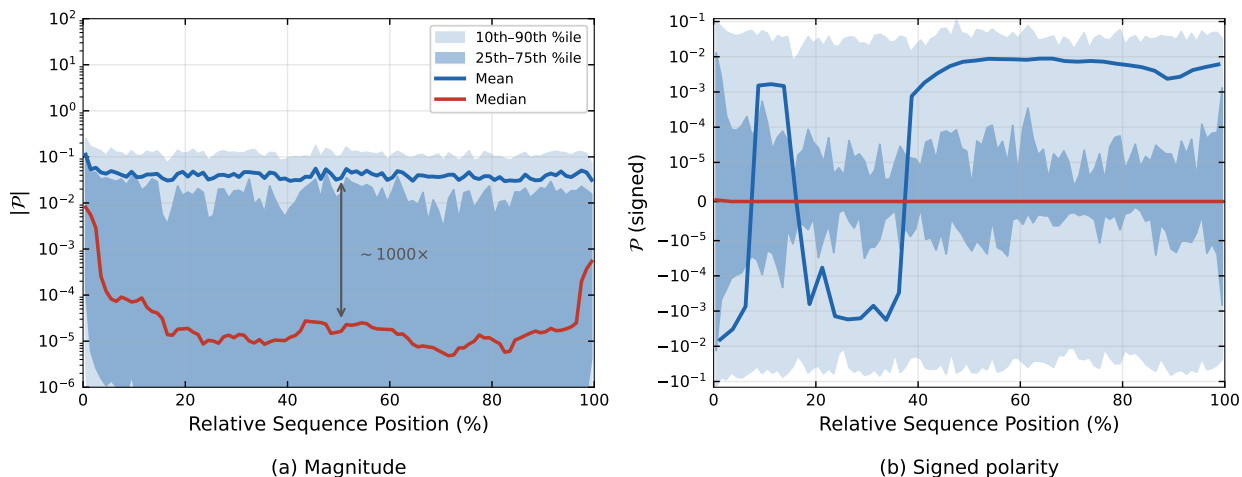


Figure 8 | Positional distribution of entropy polarity \mathcal{P} . Shaded bands show the 10th–90th and 25th–75th percentile ranges; solid lines show mean (blue) and median (red). (a) Magnitude $|\mathcal{P}|$: the mean remains flat while the median sits $\sim 1000\times$ lower, reflecting heavy-tail sparsity at every position. (b) Signed \mathcal{P} : the mean transitions from net contraction in early positions to net expansion in later positions, while the median remains at zero.

informative gradient signal at every location, whereas polarity-based selection captures the sparse, high-impact tokens regardless of where they appear.

Signed polarity reveals a positional trend. The signed mean transitions from net negative (contraction-dominated) in the first $\sim 15\%$ of the sequence to net positive (expansion-dominated) thereafter, while the median remains at zero throughout. This pattern admits a natural interpretation: early tokens in reasoning chains typically establish the solution direction (e.g., selecting a proof strategy or computation framework) and tend to be high-confidence, so reinforcement concentrates probability further and produces a contracting effect. Later tokens handle more uncertain, problem-specific reasoning steps where the model distributes probability more broadly, yielding a net expansion tendency. The near-zero median confirms that expansion and contraction tokens are balanced in count at every position; the directional bias arises solely from the magnitude-weighted tail, consistent with the heavy-tail structure observed in panel (a).

C.2. Complete Training Dynamics

Qwen2.5-7B-Base (Math). Figure 9 shows the full training curves for all four methods on the 7B backbone. The overall trends mirror the 14B results in Figure 5: PAPO achieves the highest final reward with a stable entropy trajectory. Unlike at 14B, PAPO’s entropy settles slightly below DAPO, suggesting that the smaller model naturally favors a more exploitative regime; crucially, entropy remains stable without collapse, indicating sufficient exploratory capacity for continued learning. The adaptive weights ω exhibit the same transient rebalancing pattern observed at 14B scale.

Qwen2.5-14B-Instruct (Agentic). Figure 10 presents the training dynamics for the agentic setting. Unlike math reasoning, the adaptive weights consistently favor the contracting branch ($\omega_{\text{neg}} > \omega_{\text{pos}}$), reflecting the more constrained action space of structured tool-call generation where exploitation is naturally preferred.

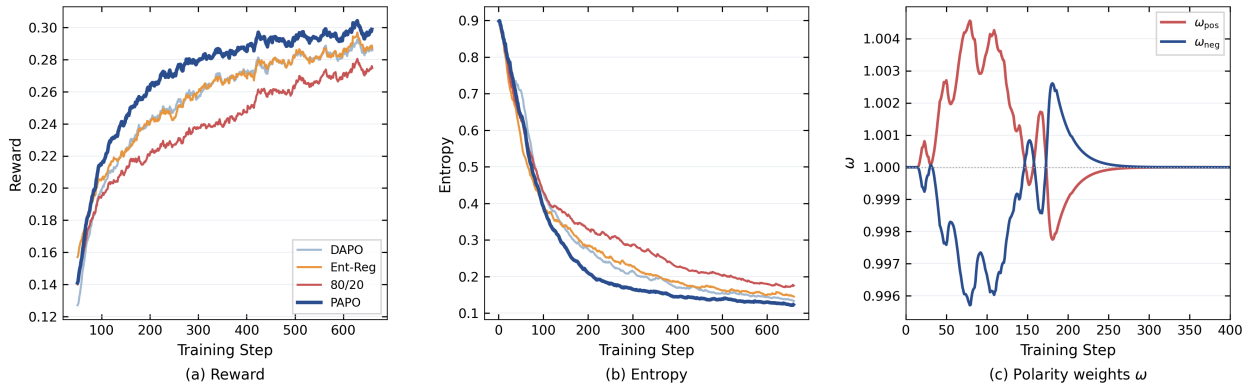


Figure 9 | Training dynamics on Qwen2.5-7B-Base (Math). (a) Reward, (b) entropy, and (c) polarity weights ω for all methods trained on DAPO-Math-17k. Trends are consistent with the 14B results in Figure 5.

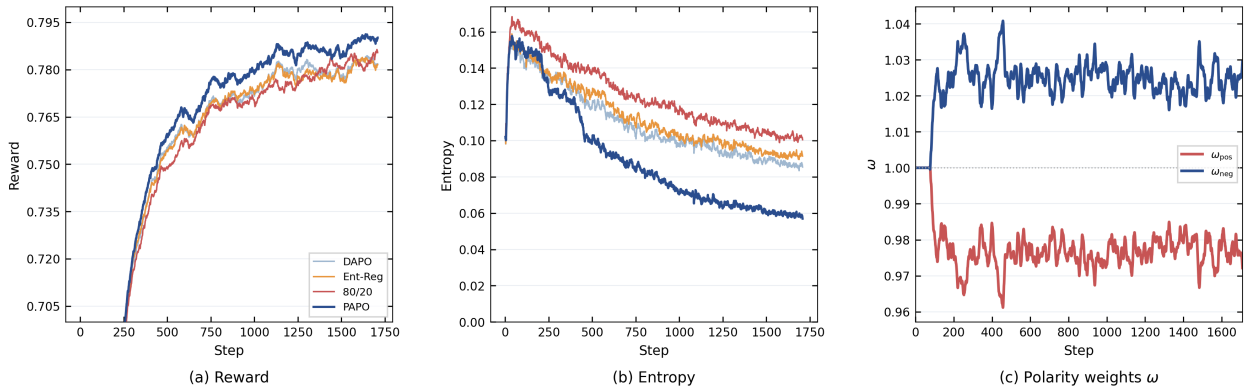


Figure 10 | Training dynamics on tool-call reasoning (Qwen2.5-14B-Instruct). (a) Reward, (b) entropy, and (c) polarity weights ω . The adaptive weights consistently favor the contracting branch, reflecting the more constrained action space of structured tool-call generation.

C.3. Detailed Out-of-Domain Results

Table 2 reports per-benchmark OOD results for all methods at both scales. All models are trained exclusively on DAPO-Math-17k and evaluated zero-shot on code reasoning, instruction following, and general knowledge benchmarks.